Quantum Diffusion on Molecular Tubes: Universal Scaling of the 1D to 2D Transition

Chern Chuang,[1] Chee Kong Lee,[1] Jeremy M. Moix,[1] Jasper Knoester,[2] and Jianshu Cao[1,*]
[1]Department of Chemistry, Massachusetts Institute of Technology, Cambridge, Massachusetts 02139, USA
[2]Zernike Institute for Advanced Materials, University of Groningen, Nijenborgh 4, 9747 AG Groningen, Netherlands
(Received 19 November 2015; revised manuscript received 23 February 2016; published 11 May 2016)

The transport properties of disordered systems are known to depend critically on dimensionality. We study the diffusion coefficient of a quantum particle confined to a lattice on the surface of a tube, where it scales between the 1D and 2D limits. It is found that the scaling relation is universal and independent of the temperature, disorder, and noise parameters, and the essential order parameter is the ratio between the localization length in 2D and the circumference of the tube. Phenomenological and quantitative expressions for transport properties as functions of disorder and noise are obtained and applied to real systems: In the natural chlorosomes found in light-harvesting bacteria the exciton transfer dynamics is predicted to be in the 2D limit, whereas a family of synthetic molecular aggregates is found to be in the homogeneous limit and is independent of dimensionality.

DOI: 10.1103/PhysRevLett.116.196803

Introduction.—Transport of energy or charge carriers is of fundamental importance in terms of both scientific interest and its technological relevance. The seminal work of Anderson states that the presence of static disorder leads to a metal-to-insulator transition or even totally prevents transport in lower dimensions [1,2]. Upon coupling to fluctuating environment, localized quasiparticles can overcome energetic barriers, and the system becomes conductive again [3]. While transport ceases to exist in both the zero coupling limit (Anderson localization) and the strong coupling limit (dynamical localization), the intervention of environmental noise with intermediate strength can maximize the conductivity [4–6].

Compared to classical hopping kinetics, where the governing rate equations are given in the coordinate basis, the motion of quantum particles on a disordered and noisy lattice is more involved. In fact, in the weak system-environment coupling limit, the dynamics of the particle wave function can be cast into rate equations in the eigenbasis. This implies that quantum enhancement of the conductivity can be characterized by the average size of the wave functions, the localization length, since this corresponds to the step size of each hopping event [6,7]. An immediate consequence arises if one considers the different scaling behaviors of the localization length in different dimensions. It is expected that, for example, the quantum enhancement is much stronger in 2D with respect to that in 1D, given the same disorder and noise strength.

In this Letter, we investigate the diffusive dynamics of a quantum particle on a tubular lattice in the axial direction, in which the transport properties scale between the 1D and the 2D limits. Recently, the optical and dynamic properties of excitons in natural [8–10] and synthetic [11–16] self-assembled tubular molecular aggregates have drawn much attention. The combination of their quasi-one-dimensional (wirelike) structure and the attenuation of exciton localization due to their inherent (locally) 2D nature, makes such tubular aggregates potentially ideal for exciton transport in, for instance, photovoltaic devices [17]. A natural order parameter in this regard is the radius of the tube, where the axial conductivity is found to be an increasing function of the radius until a critical radius is reached and levels off as it approaches the 2D limit. We found that the scaling relation is universal, independent of the parameters chosen. Moreover, the critical radius is shown to be directly proportional to the localization length in the corresponding 2D system. A phenomenological expression is proposed and shown to reproduce the radius dependence quantitatively, which is applied to several real systems in different limiting parameter regimes and predicts their respective radius-(in)dependent diffusion constant.

Calculation of quantum diffusion.—The Haken-Strobl-Reineker (HSR) model is employed to characterize the system of interest coupled to a classical Markovian noisy environment [18–20]. The dynamics of the system is described by the stochastic Schrödinger equation (taking $\hbar = 1$)

$$i\frac{d}{dt}|\psi\rangle = \hat{H}_s|\psi\rangle + \sum_{\mathbf{n}} F_{\mathbf{n}}(t)\hat{V}_{\mathbf{n}}|\psi\rangle, \tag{1}$$

where $\hat{V}_{\mathbf{n}} = |\mathbf{n}\rangle\langle\mathbf{n}|$, $F_{\mathbf{n}}(t)$ are Gaussian stochastic processes with zero mean ($\langle F_{\mathbf{n}}(t)\rangle = 0$) and finite second order autocorrelation $\langle F_{\mathbf{n}}(t)F_{\mathbf{m}}(s)\rangle = \Gamma\delta_{\mathbf{nm}}\delta(t-s)$, with Γ the dephasing rate. The system Hamiltonian $\hat{H}_s$ is characterized by a nearest-neighbor coupled square lattice with a periodic boundary condition in one direction (circumference) and isotropic coupling constant J. The number of sites (R) along the tube's circumference is referred to as the radius of the tube. The energy of site $\mathbf{n}$, $\epsilon_{\mathbf{n}}$, is taken to be an

independent Gaussian random variable with standard deviation σ.

The central physical observable in this Letter, the diffusion coefficient D in the direction along unit vector $\mathbf{u}$, is given by the Green-Kubo expression

$$D(\mathbf{u}) = \frac{1}{Z_s}\int_0^\infty dt \mathrm{Tr}[e^{-\beta \hat{H}_s}\hat{j}(\mathbf{u},t)\hat{j}(\mathbf{u})], \tag{2}$$

where Z_s is the system partition function. In the context of the HSR model, we will take $\beta = 0$ (infinite temperature), so $Z_s = N$, where N is the size of the system. The time integration can be carried out analytically.

$$D(\mathbf{u}) = \frac{1}{N}\sum_{\mu,\nu=1}^{N} \frac{\Gamma}{\Gamma^2 + \omega_{\mu\nu}^2}|\hat{j}_{\mu\nu}(\mathbf{u})|^2, \tag{3}$$

where $\hat{j}_{\mu\nu}(\mathbf{u})$ is the flux operator in the eigenbasis and $\omega_{\mu\nu} = \omega_\mu - \omega_\nu$ is the energy difference between eigenstates μ and ν. See detailed derivations in the Supplemental Material [21]. It typically takes up to 100 sites in the axial direction to converge the results for the range of disorder strength covered in this Letter. The diffusion coefficient obtained through Eq. (3) is quantitatively agreeing with that from propagating Eq. (1) as was done in Ref. [6]. For consistency, in this Letter, we present the data obtained with Eq. (3) exclusively. An efficient method of propagating Eq. (1) in the weak coupling regime ($\Gamma/J \ll 1$) is also presented in the Supplemental Material [21]. The same methodology is applicable to the case where the system is weakly coupled to a real quantum bath in the low temperature regime, as elaborated in later sections.

The present model is exactly solvable in two limiting cases. First, the dynamics of a homogeneous system ($\sigma = 0$) can be solved analytically and shows transient ballistic behavior before transitioning to diffusive motion [6,19]. The dynamics is independent of dimensionality, and the diffusion coefficient is given by [7]

$$D_{\mathrm{hom}} = 2J^2/\Gamma, \tag{4}$$

which can be obtained by assuming Bloch wave functions $\phi_m^\mu = \exp(i\mu m)/\sqrt{N}$ in Eq. (3). In fact, decoupling of directions is valid as long as the wave functions of the system can be factorized: $\Psi(\mathbf{n}) = \psi(n_1)\psi(n_2)\cdots\psi(n_M)$. One such example is given by stacks of homogeneous rings with energy bias among different rings [22,23]. In the opposite extreme, where either disorder ($\sigma/J \gg 1$) or system-environment coupling ($\Gamma/J \gg 1$) is large, all quantum coherence is destroyed. The particle behaves classically and can be described by a hopping rate between connected sites [24–26]

$$D_{\mathrm{hop}} = \frac{2J^2\Gamma}{\Gamma^2 + \sigma^2}. \tag{5}$$

Since the hopping events are independent along different directions, independence on dimensionality is also expected. We conclude that prominent radius dependence is expected only if the wave functions are nonseparable and with finite noise strength.

In the weak damping regime with finite disorder, through a scaling argument, one can show that the diffusion coefficient can be estimated by

$$D_{\mathrm{coh}} = \Gamma\xi^2, \tag{6}$$

where ξ is the localization length. This relation is very useful since it connects the dynamical observable (diffusion coefficient) with a static property of the system and a single parameter characterizing the system-environment coupling [4,6], as will be exploited in the following section. We provide the detailed derivation of Eqs. (3), (4), and a heuristic derivation of Eq. (6) in the Supplemental Material [21].

Numerical results.—We start by discussing the diffusion constants in 1D and 2D. It has been shown that the localization length scales linearly with the mean free path in 1D and exponentially in 2D [27]. A common and useful measure of the localization length is given by the inverse participation ratio (IPR), defined for each of the eigenstates as $\mathrm{IPR}_\mu = 1/\sum_{\mathbf{m}}|\phi_{\mathbf{m}}^\mu|^4$. Because of the high temperature characteristic of the HSR model, we average over all eigenstates and fit the IPR of disordered 1D and 2D square lattices according to

$$\xi^{1\mathrm{D}} = \mathrm{IPR}^{1\mathrm{D}} \sim a_1 l, \tag{7}$$

$$(\xi^{2\mathrm{D}})^2 = \mathrm{IPR}^{2\mathrm{D}} \sim a_2 l \exp(b_2 l), \tag{8}$$

where $l = (J^2/\sigma^2)$ is the mean free path, and the length scale is measured in units of the lattice constant. The results are shown in Fig. 1(a). These expressions provide a simple way of estimating the diffusion coefficient in the weak damping regime given the disorder strength σ, where Eq. (6) applies. Note that, in 1D, the IPR is directly interpreted as the localization length while, in 2D, its square root is. This is because it is the diffusion along one particular direction that concerns us.

Thouless and Kirkpatrick proposed an interpolating formula for the general case which was proven to be valid for most of the parameter range of interest [3,6]

$$D_{\mathrm{interp}} = \left[\left(\frac{2J^2}{\Gamma + \sigma/2}\right)^{-1/2} + (\Gamma\xi^2)^{-1/2}\right]^{-2}. \tag{9}$$

In Fig. 1(b), this interpolation result is shown as a function of Γ and compared to the numerically exact results obtained from Eq. (3), averaging over 100 realizations of disorder. At a given disorder strength σ, one expects an optimal dephasing rate maximizing transport [6,28]. The

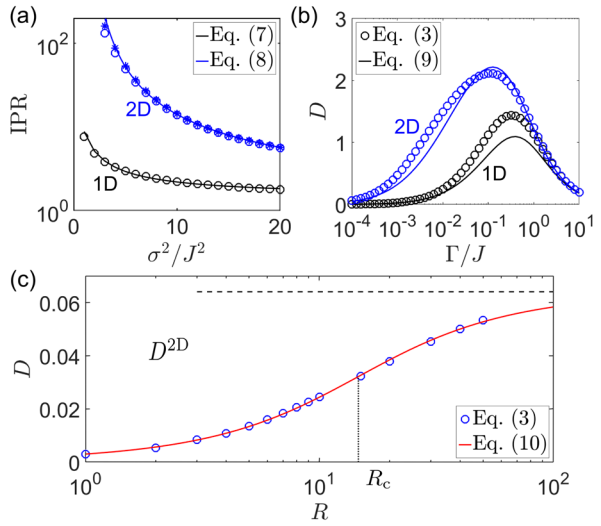

FIG. 1. (a) IPR dependence on the disorder strength in 1D and 2D. The parameters fitted in Eqs. (7) and (8) (solid lines) are $a_1 = 6.2$ and $(a_2, b_2) = (67, 6.7)$. The numerical data are shown in symbols. We use 4900 sites for 1D system (black circles), and 2D systems with 70×70 (blue circles) and 90×90 (blue asterisks) square lattices. (b) Comparison between the results of Eq. (3) and those of Eq. (9). The lower (black) circles and solid line refer to 1D systems and the upper (blue) circles and line represent 2D systems. In both cases, we set $\sigma/J = 1$. (c) Radius dependence of D with $\sigma/J = 1$ and $\Gamma/J = 10^{-4}$. The solid line is the fitting according to Eq. (10), with the corresponding fitted parameters R_c and D^{2D} indicated.

interpolation formula not only describes the two limits correctly, but also captures the maxima almost quantitatively, showing the transition between the two transport mechanisms. Note that this expression also reproduces the convergence of diffusion constants in different dimensions in the homogeneous limit, i.e., Eq. (4).

Next, we look at the radius dependence of the diffusion constant in a tube. Since the diffusive motion in the large dephasing limit is independent of dimensionality, and the Γ dependence is well described by Eq. (9), we will focus on the Redfield regime ($\Gamma/J \ll 1$) while the effect of finite Γ is analyzed in the Supplemental Material [21]. This dependence should be bounded from below by the results of 1D diffusion and from above by 2D diffusion, as seen in Fig. 1(c). The diffusion constant increases as the tube radius R increases until the trend is attenuated at the inflection point $R = R_c$, denoted as the critical radius. This radius dependence is universal across the entirety of the parameter space we scanned, as shown in Fig. 2, where the data are rescaled according to the phenomenological expression

$$D(R) = D^{1D} + (D^{2D} - D^{1D}) S\left(\frac{R-1}{R_c}\right), \qquad (10)$$

where $S(0) = 0$, $S(\infty) = 1$, and dS/dx is everywhere positive for $x > 0$. Here, we chose $S(x) = 2\arctan(x)/\pi$

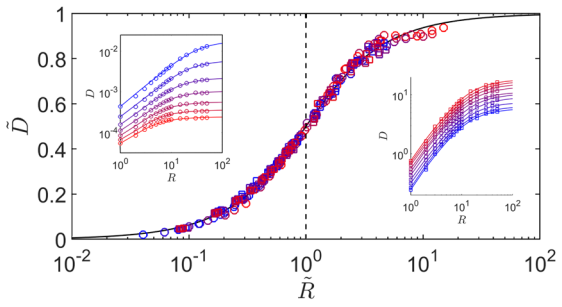

FIG. 2. Relative diffusion coefficient $\tilde{D} = [D(R) - D^{1D}]/(D^{2D} - D^{1D})$ as a function of rescaled radius $\tilde{R} = (R-1)/R_c$. The solid line is the fitting function $S(x)$ and the dashed line indicates $\tilde{R} = 1$. Inset (left) shows data from Eq. (3) before rescaling: From top ($\sigma/J = 2$, blue) to bottom ($\sigma/J = 5$, red) with 0.5 increment and interpolating color gradient. Inset (right) shows data from the quantum bath calculations with varying temperatures: From top ($T/J = 7$, red) to bottom ($T/J = 0.7$, blue) with 0.7 decrement.

[29]. To demonstrate the generality of this observation, we also present the universality found for systems with a realistic quantum bath treated under the secular Redfield approximation (right inset, Fig. 2). With the details described in the Supplemental Material [21], this method accurately models the low temperature thermal activated transport regime that complements the HSR model [30,31], as indicated by the linearly spaced curves on the log-log scaled right inset of Fig. 2. This exponential regime bridges the temperature independent regime near zero temperature and linearly scaling regime at moderate temperature shown in our previous study [7]. The model has also been shown to explain the temperature dependent exciton properties of molecular aggregates relevant to our discussion in the next section [32,33].

The universality can be explained by the following interpretation. One expects a strong radius dependence of the diffusion coefficient only if the particle wave function fully delocalizes around the tube. This is no longer valid as the radius becomes larger than its critical value, where the wave function only partially occupies the space in the circumferential direction. Essentially, this picture identifies the critical radius with the localization

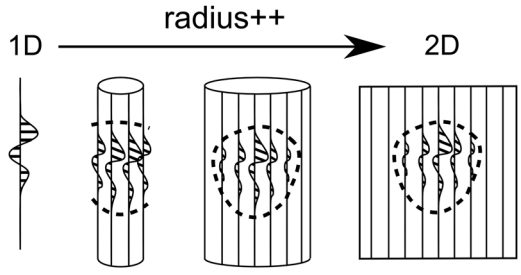

FIG. 3. Schematic illustration of the origin of universal radius scaling of transport rate in tubes.

length in the corresponding 2D system, as is illustrated in Fig. 3. In determining the radius dependence, one compares two length scales of the system: the circumference of the tube and the inherent localization length along the circumference. This makes our theory predictive on the axial diffusion coefficients of general tubular systems, given the knowledge of the localization length obtained from experiments or *ab initio* calculations, as demonstrated in the next section. We note that this picture can also be applied to understanding the optical selection rules for the dichroism spectra of tubular systems [34].

Estimates for real systems.—There are numerous examples of exciton transport in tubular aggregates consisting of organic chromophores. Amongst the best known examples found in nature are the chlorosomes in green sulfur bacteria [8], which serve as the antenna of the light-harvesting apparatus. Diffusive transport of excitons in chlorosomes has been identified [35,36]. The above scaling argument predicts the exciton diffusion on chlorosome tubes to be in the 2D limit, because the critical radius R_c is much smaller than the typical radius found in the organism, see Table I [37]. This implies that the chlorosomes fully exploit the enhancement and robustness of quantum transport in 2D compared to 1D, while taking the advantage of a broad absorption spectrum induced by strong homogeneous (Γ) and inhomogeneous (σ) broadening mechanisms [38].

Families of synthetic self-assembled tubular molecular aggregates exist as well, mimicking chlorosomes with axial length up to the micron scale [11,41,42]. One such aggregate, composed of the dye molecule C8S3, has been recently characterized [14,43]. Because of the reduced static disorder and strong exciton coupling strength ($J \approx 8\sigma$, see Table I), the system is in the homogeneous limit and the diffusion coefficient becomes independent of dimensionality or radius. This conclusion is supported by the well-defined absorption selection rules arising from the wave functions fully delocalized around the circumferences [14,41]. The large localization length in such systems can be utilized in transporting the excitons efficiently along the tubes [17,43].

There are other instances where radius (in)dependence of transport in tubular systems is seen. It has been shown that the exciton mobility in semiconducting single-walled carbon nanotubes increases linearly with the radius [44]. This implies that the reduced disorder in clean carbon nanotube samples gives rise to large localization length [45], so the system is in the $R \ll R_c$ limit that shows linear radius dependence. In addition, molecular tubes based on tobacco mosaic virus protein monomers designed to mimic natural light-harvesting arrays were synthesized [46]. It is found that the exciton dynamics can be described appropriately by classical hopping kinetics [40,47]; thus, the independence of dimensionality is predicted (see Table I). Last, quantum diffusion of excitons in aggregated phycocyanin thin films has been experimentally characterized recently [48], where the delocalization of excitons explains the enhancement of the diffusion length compared to the estimate of classical hopping theory. While this artificial system serves as an example of quantum diffusion in 2D, the naturally occurring form of phycocyanin in most cyanobacteria self-assembles into a finite 1D wire [49]. It is our ongoing effort to analyze this interesting system in this regard.

Both the HSR model and the secular Redfield method applied to isotropic nearest-neighbor coupled square lattices are an oversimplification of the real systems [37]. Richer physical content can be expected when considering more realistic aspects. For example, it has been shown that environmental memory effects can enhance diffusive transport [25,36]. The anisotropy from nontrivial molecular arrangement could, for example, render a helical character to the exciton wave function [34,50–52]. Moreover, the statistics of disorder [53] and long-range interactions [54] are both critical in determining the localization length. We expect the R dependence to be more involved in these and other possible generalizations, since the functional dependence of the localization length on the additional model parameters varies. However, once given these parameters and, thus, the localization length, the transition from 1D to 2D can be compactly characterized by the ratio between the radius and the localization length. Consequently, we believe the universal scaling relation investigated in this Letter can serve as a generic guidance. Finally, the theoretical framework developed here also applies to, for

TABLE I. Parameters and axial exciton diffusion estimated [37] for three exemplary real tubular systems at room temperature. J, σ, Γ are given in cm^{-1}, diffusion coefficients are in $\mathrm{nm}^2/\mathrm{ps}$, and R (R_c) is unitless representing the (critical) number of molecules in the circumference. The parameters for J, σ, Γ, and R from top to bottom are deduced from Refs. [36], [39], [14], and [40], respectively. The other quantities are calculated using Eqs. (7), (8), and (9). We take $R_c = \xi^{2D}$ since the ratio between ξ^{2D} from Eq. (8) and the fitted R_c from Eq. (10) are close to unity in our calculations.

	J	σ	Γ	D^{1D}	D^{2D}	R_c	R
Chlorosome	400	1000	350	26	35	6	100
C8S3 tube	2000	250	300	2800	2900	⋯	30/60
TMV tube[a]	50	3000	400	0.6	0.6	1	17

[a]Tobacco mosaic virus.

example, the in-plane exciton mobility as a function of the thickness of thin films, which is predicted to scale between the 2D and the 3D limits.

Conclusion.—We have developed a theoretical framework and efficient numerical procedure to model exciton dynamics in tubular molecular aggregates in the presence of environmental noise and disorder based on the HSR model and the secular Redfield model. The central observation is that the diffusion coefficient along the axial direction increases as a function of the tube radius. This dependence is found to be universal across the full parameter range of interest, and can be succinctly characterized by the ratio between the tube circumference and the localization length of the corresponding 2D system. For the chlorosome tubes found in green sulfur bacteria, the exciton transport is found to be in the 2D limit. On the other hand, in a synthetic system with self-assembled cyanine dye molecules mimicking chlorosomes, the excitons are in the homogeneous limit where independence of dimensionality is predicted. Our findings are useful when exploiting the structure-property relation in designing robust and efficient artificial light-harvesting devices.

This work is supported by the NSF (Grant No. CHE-1112825) and the Singapore-MIT Alliance for Research and Technology (SMART).

*jianshu@mit.edu

[1] P. W. Anderson, Phys. Rev. **109**, 1492 (1958).
[2] E. Abrahams, P. W. Anderson, D. C. Licciardello, and T. V. Ramakrishnan, Phys. Rev. Lett. **42**, 673 (1979).
[3] D. J. Thouless and S. Kirkpatrick, J. Phys. C **14**, 235 (1981).
[4] D. A. Evensky, R. T. Scalettar, and P. G. Wolynes, J. Phys. Chem. **94**, 1149 (1990).
[5] D. M. Leitner and P. G. Wolynes, Phys. Rev. Lett. **76**, 216 (1996).
[6] J. M. Moix, M. Khasin, and J. Cao, New J. Phys. **15**, 085010 (2013).
[7] C. K. Lee, J. Moix, and J. Cao, J. Chem. Phys. **142**, 164103 (2015); Herein three different temperature regimes were classified under a unified polaron framework: classical hopping, band-like, and zero-point fluctuations.
[8] S. Ganapathy, G. T. Oostergetel, P. K. Wawrzyniak, M. Reus, A. G. M. Chew, F. Buda, E. J. Boekema, D. A. Bryant, A. R. Holzwarth, and H. J. M. de Groot, Proc. Natl. Acad. Sci. U.S.A. **106**, 8525 (2009).
[9] M. Jendrny, T. J. Aartsma, and J. Kohler, J. Phys. Chem. Lett. **3**, 3745 (2012).
[10] Y. Tian, R. Camacho, D. Thomsson, M. Reus, A. R. Holzwarth, and I. G. Scheblykin, J. Am. Chem. Soc. **133**, 17192 (2011).
[11] T. G. Barclay, K. Constantopoulos, and J. Matisons, Chem. Rev. **114**, 10217 (2014).
[12] S. M. Vlaming, R. Augulis, M. C. A. Stuart, J. Knoester, and P. H. M. van Loosdrecht, J. Phys. Chem. B **113**, 2273 (2009).
[13] A. Pawlik, S. Kirstein, U. De Rossi, and S. Daehne, J. Phys. Chem. B **101**, 5646 (1997).
[14] D. M. Eisele, C. W. Cone, E. A. Bloemsma, S. M. Vlaming, C. G. F. van der Kwaak, R. J. Silbey, M. G. Bawendi, J. Knoester, J. P. Rabe, and D. A. Van den Bout, Nat. Chem. **4**, 655 (2012).
[15] K. A. Clark, C. W. Cone, and D. A. Van den Bout, J. Phys. Chem. C **117**, 26473 (2013).
[16] D. Abramavicius, A. Nemeth, F. Milota, J. Sperling, S. Mukamel, and H. F. Kauffmann, Phys. Rev. Lett. **108**, 067401 (2012).
[17] E. A. Bloemsma, S. M. Vlaming, V. A. Malyshev, and J. Knoester, Phys. Rev. Lett. **114**, 156804 (2015).
[18] V. M. Kenkre and P. Reineker, *Exciton Dynamics in Molecular Crystals and Aggregates* (Springer, New York, 1982).
[19] A. Madhukar and W. Post, Phys. Rev. Lett. **39**, 1424 (1977).
[20] A. Amir, Y. Lahini, and H. B. Perets, Phys. Rev. E **79**, 050105 (2009).
[21] See Supplemental Material at http://link.aps.org/supplemental/10.1103/PhysRevLett.116.196803 for the derivations and details of the simulations.
[22] M. J. McIntire, E. S. Manas, and F. C. Spano, J. Chem. Phys. **107**, 8152 (1997).
[23] C. Chuang, J. Knoester, and J. Cao, J. Phys. Chem. B **118**, 7827 (2014).
[24] J. Cao and R. J. Silbey, J. Phys. Chem. A **113**, 13825 (2009).
[25] J. Wu, F. Liu, Y. Shen, J. Cao, and R. J. Silbey, New J. Phys. **12**, 105012 (2010).
[26] J. Wu, R. J. Silbey, and J. Cao, Phys. Rev. Lett. **110**, 200402 (2013).
[27] P. A. Lee and T. V. Ramakrishnan, Rev. Mod. Phys. **57**, 287 (1985).
[28] L. Cleary and J. Cao, New J. Phys. **15**, 125030 (2013).
[29] The numerical evaluation of Eq. (3) is demanding for 2D lattices. We fix the number of sites in the axial direction to 100, with sites on the circumference up to 50. Both D^{2D} and R_c are fitted according to Eq. (10).
[30] B. Movaghar, M. Grünewald, B. Ries, H. Bässler, and D. Würtz, Phys. Rev. B **33**, 5545 (1986).
[31] H. Bässler, Phys. Status Solidi B **175**, 15 (1993).
[32] M. Bednarz, V. A. Malyshev, and J. Knoester, Phys. Rev. Lett. **91**, 217401 (2003).
[33] D. J. Heijs, V. A. Malyshev, and J. Knoester, Phys. Rev. Lett. **95**, 177402 (2005).
[34] S. M. Vlaming, E. A. Bloemsma, M. L. Nietiadi, and J. Knoester, J. Chem. Phys. **134**, 114507 (2011).
[35] J. Dostal, T. Mancal, R. Augulis, F. Vacha, J. Psencik, and D. Zigmantas, J. Am. Chem. Soc. **134**, 11611 (2012).
[36] T. Fujita, J. C. Brookes, S. K. Saikin, and A. Aspuru-Guzik, J. Phys. Chem. Lett. **3**, 2357 (2012).
[37] We use an effective nearest-neighbor coupling which accounts the same bandwidth as a 2D dipolar lattice. The dephasing rate Γ is estimated by taking the fast bath limit of a quantum bath such that the bath correlation function becomes a δ function, e.g., $\Gamma \approx 2\lambda/\beta\omega_c$ for a Drude-Lorentz bath $J(\omega) = 2\lambda\omega_c\omega/(\omega_c^2 + \omega^2)$
[38] We note that the chlorosome tubes lie horizontally on the baseplate above the Fenna-Matthews-Olson complexes and the reaction centers. However, the 2D enhancement of quantum diffusion applies to the circumferential transport as well. Also, under high photon influx, the excitons can migrate axially and reach unoccupied reaction centers.

[39] J. Sperling, A. Nemeth, J. Hauer, D. Abramavicius, S. Mukamel, H. F. Kauffmann, and F. Milota, J. Phys. Chem. A **114**, 8179 (2010).
[40] M. Sarovar and K. B. Whaley, New J. Phys. **15**, 013030 (2013).
[41] C. Didraga, A. Pugzlys, P. Hania, H. von Berlepsch, K. Duppen, and J. Knoester, J. Phys. Chem. B **108**, 14976 (2004).
[42] Y. Wan, A. Stradomska, S. Fong, Z. Guo, R. D. Schaller, G. P. Wiederrecht, J. Knoester, and L. Huang, J. Phys. Chem. C **118**, 24854 (2014).
[43] K. A. Clark, E. L. Krueger, and D. A. Van den Bout, J. Phys. Chem. Lett. **5**, 2274 (2014).
[44] A. J. Siitonen, D. A. Tsyboulski, S. M. Bachilo, and R. B. Weisman, J. Phys. Chem. Lett. **1**, 2189 (2010).
[45] A. V. Narlikar and Y. Y. Fu, eds., *Oxford Handbook of Nanoscience and Technology: Frontiers and Advances* (Oxford University Press, New York, 2009).
[46] R. A. Miller, A. D. Presley, and M. B. Francis, J. Am. Chem. Soc. **129**, 3104 (2007).
[47] J. H. Kim and J. Cao, J. Phys. Chem. B **114**, 16189 (2010).
[48] I. Eisenberg, S. Yochelis, R. Ben-Harosh, L. David, A. Faust, N. Even-Dar, H. Taha, N. M. Haegel, N. Adir, N. Keren, and Y. Paltiel, Phys. Chem. Chem. Phys. **16**, 11196 (2014).
[49] C. Theissa, F.-J. Schmitta, J. Pieperb, C. Nganoua, M. Grehn, M. Vitali, R. Olliges, H. J. Eichler, and H.-J. Eckert, Journal of plant physiology **168**, 1473 (2011).
[50] F. Dominguez-Adame, V. A. Malyshev, and A. Rodriguez, J. Chem. Phys. **112**, 3023 (2000).
[51] L. Cleary, H. Chen, C. Chuang, R. J. Silbey, and J. Cao, Proc. Natl. Acad. Sci. U.S.A. **110**, 8537 (2013).
[52] A. G. Dijkstra, H. G. Duan, J. Knoester, K. A. Nelson, and J. Cao, J. Chem. Phys. **144**, 134310 (2016).
[53] S. M. Vlaming, V. A. Malyshev, and J. Knoester, Phys. Rev. B **79**, 205121 (2009).
[54] A. V. Malyshev and V. A. Malyshev, Phys. Rev. B **63**, 195111 (2001).